



**IV Congresso Nacional de Engenharia Mecânica
22 a 25 de Agosto 2006, Recife-PE**

A NUMERICAL STUDY OF THE COMPRESSIBILITY EFFECT ON FLOWFIELD STRUCTURE OF BLUNT BODIES IN LOW-DENSITY FLOW

Wilson F. N. Santos

Wilson@lcp.inpe.br

Combustion and Propulsion Laboratory
National Institute for Space Research
Cachoeira Paulista, SP 12630-000

***Abstract.** Hypersonic flow over flat-nose leading edges is examined for a range of freestream Mach number from 5 to 12 at zero-incidence. The work is motivated by interest in assessing the overall performance of flat-nose leading edges in order to consider them as possible candidates for blunting geometries of hypersonic configurations. The Direct Simulation Monte Carlo (DSMC) method has been employed in order to examine the flowfield structure around these leading edges. A very detailed description of the primary flow property behavior at the vicinity of the leading edge noses and immediately adjacent to the afterbody surfaces has been presented. The results presented highlight some significant differences on the flowfield properties due to variations on the flat-face thickness of the leading edges and on the freestream Mach number. Interesting features observed in the primary properties showed that small flat-face thickness, compared to the freestream mean free path, still has important effects on high Mach number leading edge flows.*

Keywords: DSMC, Hypersonic Flow, Rarefied Flow, Blunt Body, Compressibility

1. INTRODUCTION

An efficient design of future airbreathing hypersonic vehicle will depend on high-lift low-drag configurations in order to overcome the aerodynamic forces involved in high-speed flight. In this context, waveriders (Nonweiler, 1959) have been considered as one of the promising vehicle concepts under consideration. Waveriders are vehicles designed so that the bow shock is everywhere attached to the sharp leading edge. Nevertheless, actual flight vehicle will include some degree of bluntness, either dictated by manufacturing requirements or by heating requirements. The latter is especially important given that heating rate on rounded edges (circular cylinder) scales inversely with the square root of the stagnation point radius, so that there is an unavoidable compromise between aerodynamic performance and heating survivability. As a result, designing a hypersonic vehicle leading edge involves a tradeoff between making the leading edge sharp enough to obtain acceptable aerodynamic and propulsion efficiency and blunt enough to reduce the aerodynamic heating in the stagnation region.

Certain classes of non-circular shapes may provide the required bluntness with smaller shock separation than round leading edges, thus allowing manufacturing, and ultimately heating control, with reduced departures from ideal aerodynamic performance. The idea that such would be possible is based on the work of Reller (1957) who has presented a method of designing low heat transfer bodies. The method is devised on the premise that the rate of heat transfer to the nose will be low if the local velocity is low, while the rate of heat transfer to the afterbody will be low if the local density is low. A typical body that results from this design method consists of a flat nose followed by a highly curved, but for the most part slightly inclined, afterbody surface.

In this connection, flat-nose leading edges (Santos, 2003, 2004 and 2005) have been considered as especially promising bluntness for hypersonic configurations in order to provide the leading edge heating and manufacturing requirements. Santos (2003) has investigated the sensitivity of the stagnation point heating and total drag to shape variations of such leading edges. The surface temperature effect on these flat-nose leading edges has been analyzed by Santos (2004). In Santos (2005), a parametric study was performed on these flat-nose leading edges with a great deal of emphasis placed on the gas-surface interaction effects.

In continuation of the research on flat-nose leading edges, the study at hand extends the analysis presented by Santos (2003, 2004 and 2005) by examining computationally the flowfield structure on these flat-nose leading edges with a great deal of effort placed on the compressibility effects.

The present study is focused on the low-density region in the upper atmosphere, where the non-equilibrium conditions are such that traditional CFD calculations are inappropriate to yield accurate results. In such a circumstance, the DSMC method will be employed to calculate the rarefied hypersonic two-dimensional flow on the flat-nose leading edges.

2. BODY-SHAPE DEFINITION

The geometry of the leading edges considered in this work is the same as that presented in Santos (2003). The blunt shapes consist of a flat nose supplemented by an afterbody surface defined, in dimensionless form, by the following contour,

$$\bar{x} = \int_{\bar{y}=1}^{\bar{y}=\bar{y}_{\max}} \sqrt{\bar{y}^k - 1} d\bar{y} \quad \text{where} \quad \bar{x} = x/y_{\text{nose}} \quad \text{and} \quad \bar{y} = y/y_{\text{nose}}. \quad (1)$$

The blunt shapes are modeled by assuming a sharp leading edge of half angle θ with a circular cylinder of radius R inscribed tangent to the wedge. The blunt shapes are inscribed tangent to them at the same common point where they have the same slope angle. It was assumed a leading edge half angle of 10 degrees, a circular cylinder diameter of 10^{-2} m and flat-face thickness t/λ_{∞} of 0.01, 0.1 and 1, where $t = 2y_{\text{nose}}$ and λ_{∞} is the freestream mean free path. Figure (1a) illustrates this construction for the set of shapes investigated. From geometric considerations, the exponent k in Eq. (1) is obtained by matching slope on the wedge, circular cylinder and on the body shapes at the tangency point. For dimensionless thicknesses of 0.01, 0.1 and 1, the exponent k corresponds to 0.501, 0.746 and 1.465, respectively. The common body height H and the body length L are obtained in a straightforward manner. It was assumed that the leading edges are infinitely long but only the length L is considered, since the wake region behind the leading edges is not of interest in this investigation.

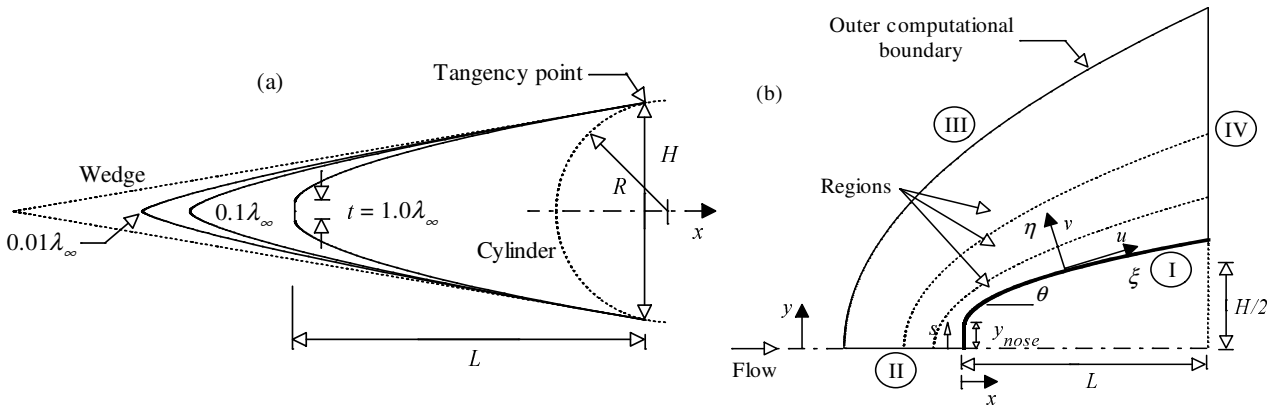


Figure 1: Drawing illustrating (a) the leading edge shapes and (b) the computational domain.

3. COMPUTATIONAL METHOD AND PROCEDURE

It is well known that the Direct Simulation Monte Carlo (DSMC) method introduced by Bird (1994) has become a reliable and efficient kinetic approach for modeling rarefied gas flows. Typical applications include high altitude rockets plumes, microelectromechanical systems (MEMS) devices, spacecraft propulsion and contamination, low-pressure plasma material-processing reactors, and reentry vehicles. Although these applications encompass a wide range of spatial and temporal scales, they are united by the same underlying physics of moderate or high Knudsen number flows. The Knudsen number Kn is the ratio of the gas mean free path λ to the characteristic length scale of the problem. It is generally accepted that the rarefied transition flow regime lies in the range of $0.01 < Kn < 10$. The transition regime is the category of flow that falls between the continuum regime, where the Navier-Stokes equations are valid, and the free molecular regime, which is the limit of infinite Knudsen number.

The DSMC method employs thousands or millions of representative molecules in order to reproduce the behavior of a far larger number of real molecules within the flow. The strategy of the method is to directly track the molecular trajectory and status, based on the collision mechanics, to model molecules in a computer and then obtain physical quantities of interest through statistical sampling. The time step has to be selected in such a way that the distance traveled by a molecule during each time step is smaller than the mean free time between collisions of the real gas (Bird, 1994).

Collisions in the present DSMC code are modeled by using the variable hard sphere (VHS) molecular model (Bird, 1981) and the no time counter (NTC) collision sampling technique (Bird, 1989). Repartition energy among internal and translational modes is controlled by the Borgnakke-Larsen statistical model (Borgnakke and Larsen, 1975). Simulations are performed using a non-reacting gas model for a constant freestream gas composition consisting of 76.3% of N_2 and 23.7% of O_2 . Energy exchanges between translational and internal modes, rotational and vibrational, are considered. Relaxation collision numbers of 5 and 50 were used for the calculations of rotation and vibration, respectively.

In the DSMC method, the physical space is divided into a certain number of cells and each cell is also divided into subcells. The physical space network is used to facilitate the choice of molecules for collisions and for the sampling of the macroscopic flow properties such as temperature, pressure, etc. In the DSMC algorithm, the linear dimensions of the cells should be small in comparison with the scale length of the macroscopic flow gradients normal to streamwise directions, which means that the cell dimensions should be of the order of or smaller than the local mean free path (Bird, 1994).

The computational domain used for the calculation is made large enough so that body disturbances do not reach the upstream and side boundaries, where freestream conditions are specified. A schematic view of the computational domain is depicted in Fig. (1b). Side I is defined by the body surface. Diffuse reflection model is the condition applied to this side. Advantage of the flow symmetry is taken into account, and molecular simulation is applied to one-half of a full configuration. Thus, side II is a plane of symmetry. In such a boundary, all flow gradients normal to the plane are zero. At the molecular level, this plane is equivalent to a specular reflecting boundary. Side III is the freestream side through which simulated molecules enter and exit. Finally, the flow at the downstream outflow boundary, side IV, is predominantly supersonic and vacuum condition is specified (Bird, 1994). At this boundary, simulated molecules can only exit.

The numerical accuracy in DSMC method depends on the cell size chosen, on the time step as well as on the number of particles per computational cell. These effects were investigated in order to determine the number of cells and the number of particles required to achieve grid independence solutions. Grid independence was tested by running the calculations with half and twice the number of cells in ξ and η directions (see Fig. 1(b)) compared to a standard grid. Solutions (not shown) were near identical for all grids used and were considered fully grid independent.

4. COMPUTATIONAL CONDITIONS

The freestream and flow conditions used in the present calculations are those given by Santos (2003) and summarized in Tab. (1). The gas properties considered in the simulation are those given by Bird (1994) and shown in Tab. (2). Referring to Tabs. (1) and (2), T_∞ , p_∞ , ρ_∞ , n_∞ , μ_∞ , and λ_∞ stand respectively for temperature, pressure, density, number density, viscosity and mean free path, and X , m , d and ω account respectively for mole fraction, molecular mass, molecular diameter and viscosity index. The freestream velocity V_∞ , assumed to be constant at 1.49, 2.37 and 3.56 km/s, corresponds to freestream Mach number M_∞ of 5, 8, and 12, respectively. The wall temperature T_w on the body surface is maintained constant at 880 K for all cases considered.

Table 1: Freestream Conditions

T_∞ (K)	p_∞ (N/m ²)	ρ_∞ (kg/m ³)	n_∞ (m ⁻³)	μ_∞ (Ns/m ²)	λ_∞ (m)
220.0	5.582	8.753×10^{-5}	1.8209×10^{21}	1.455×10^{-5}	9.03×10^{-4}

Table 2: Gas Properties

	X	m (kg)	d (m)	ω
O ₂	0.237	5.312×10^{-26}	4.01×10^{-10}	0.77
N ₂	0.763	4.650×10^{-26}	4.11×10^{-10}	0.74

The overall Knudsen number Kn_t , defined as the ratio of the freestream mean free path λ_∞ to the flat-face thickness t , corresponds to 100, 10 and 1 for leading edges with thickness t/λ_∞ of 0.01, 0.1 and 1, respectively. The Reynolds number Re_t covers the range from 0.193 to 19.3, based on conditions in the undisturbed stream with the flat-face thickness t as the characteristic length.

4. COMPUTATIONAL RESULTS AND DISCUSSION

The focus of this section is to summarize the major features of the results computed over a wide range of input conditions and simulation parameters. In this connection, the purpose of this section is to discuss and to compare differences in the flowfield properties due to variations on the flat-face thickness and on the freestream Mach number. The flowfield properties of particular interest in the transitional flow regime are velocity, density, pressure and temperature.

4.1. Velocity Profile

Distribution of normal velocity profiles along the stagnation streamline and their dependence on the freestream Mach number is illustrated in Figs. (2a-c) for leading-edge thickness corresponding to Kn_t of 100, 10 and 1, respectively. In this set of figures, the normal velocity v is normalized by the freestream velocity V_∞ , and the distance upstream the leading edges, along the body normal η -direction (see Fig. (1b)) is normalized by the freestream mean free path λ_∞ . It is important to note that V_∞ is different for each freestream Mach number case and, therefore, the comparison is made in terms of ratio.

According to these figures, it is seen that the leading edge thickness as well as the freestream Mach number influences the flowfield far upstream. This domain of influence increases with increasing the flat-face thickness of the leading edge and with decreasing the freestream Mach number. The flat-face thickness effect results from the upstream diffusion of particles that are reflected from the nose of the leading edge. Consequently, blunting the nose of the body (increasing t) leads to significantly larger disturbance upstream of the body. On the other hand, with the freestream Mach number decrease, particles reflecting from the body surface diffuse further

upstream due to the lower density at the vicinity of the leading edge nose, as will be seen subsequently. For instance, the upstream disturbance along the stagnation streamline for a velocity reduction of 1% ($v/V_\infty = 0.99$) is around $3.90\lambda_\infty$, $4.52\lambda_\infty$ and $5.68\lambda_\infty$ for cases $t/\lambda_\infty = 0.01$, 0.1 and 1 , respectively, and freestream Mach number of 5. However, it changes to around $2.73\lambda_\infty$, $3.21\lambda_\infty$ and $5.13\lambda_\infty$ for cases $t/\lambda_\infty = 0.01$, 0.1 and 1 , respectively, and freestream Mach number of 12.

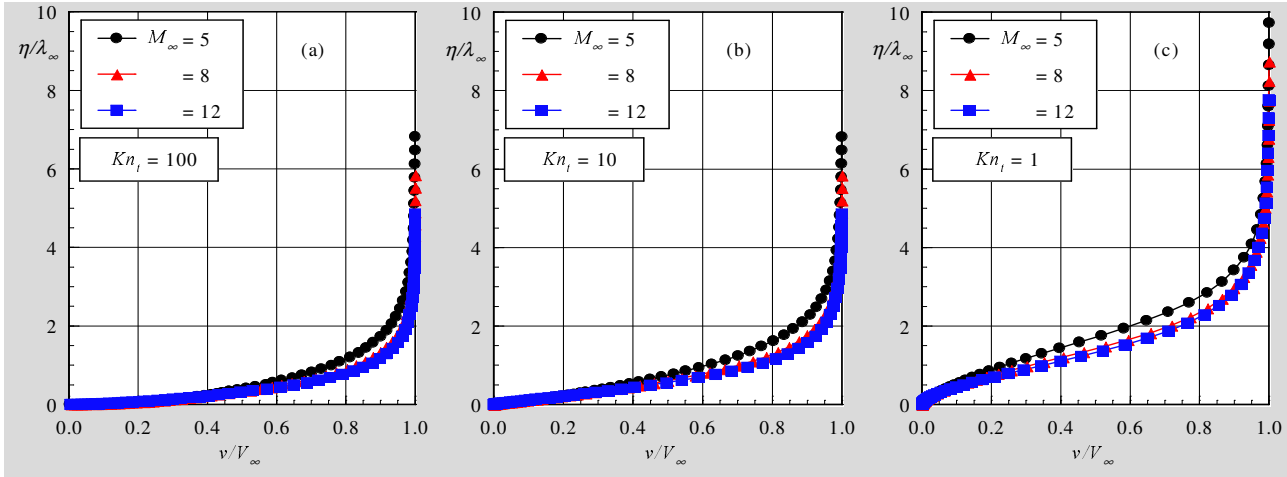


Figure 2: Normal velocity (v/V_∞) profiles along the stagnation streamline as a function of the freestream Mach number for thickness Knudsen number Kn_t of (a) 100, (b) 10 and (c) 1.

4.2. Density Profile

Density profiles along the stagnation streamline are displayed as a function of the freestream Mach number in Figs. (3a-c) for Kn_t of 100, 10 and 1, respectively. In this set of figures, density ρ is normalized by the freestream density ρ_∞ .

The predictions of density for the freestream Mach number range investigated show no sign of a discrete shock wave. It is clearly seen a continuous rise in density from the freestream to the nose of the leading edges, indicating the diffuse nature of the shock wave, a characteristic of highly rarefied flows. Also, it can be recognized that density rises to well above the continuum inviscid limit for the majority of the cases investigated. As a point of reference, the Rankine-Hugoniot relations give a postshock density that corresponds to the ratio ρ/ρ_∞ of 5.0 and 5.8 for freestream Mach numbers of 5 and 12, respectively. Near the stagnation point ($\eta/\lambda_\infty \approx 0$), a substantial density increase occurs which is a characteristic of cold-wall entry flow. In typical entry flow, the body surface temperature is low compared to the stagnation temperature. This leads to a steep density gradient near the body surface. For the present simulation, the ratio of wall temperature to stagnation temperature is 0.13, which correspond to a cold-wall flow.

By considering free molecular flow (Bird, 1994), the density ratio at the stagnation point is equal to 4.70, 6.93 and 9.89 for freestream Mach number of 5, 8 and 12, respectively. It may be recognized from the density distribution in Fig. (3a) that the density ratio for the $Kn_t = 100$ case ($t/\lambda_\infty = 0.01$ case) is approaching the free molecular value at the stagnation point. Unlike normal velocity, density has little effect on the extent of the domain of influence upstream of the body for the leading edge cases investigated. Much of the density increase in the shock layer occurs after the temperature has reached its postshock value, as will be also seen subsequently.

Variation of local density along the body normal direction, expressed as a ratio to the freestream value, is depicted in Figs. (4a-c) as a function of the freestream Mach number for the $Kn_t = 1$ case. This set of plots presents data at three afterbody stations that correspond to body slope angle of 80, 40 and 20 degrees. According to these plots, it is observed that density is affected by the freestream Mach number rise, as would be expected. Based on Fig. (4a), which corresponds to the station of 80 degrees, the density variation is in excess of one order of magnitude for freestream Mach number

cases of 8 and 12. In this region, close to the stagnation region, the compression combined with a relatively cool wall produces a maximum density that is 6.6, 12.2 and 20.7 times the freestream value for freestream Mach number cases of 5, 8 and 12, respectively. Because of the flow expansion along the afterbody surface, the density adjacent to the surface decreases to around 2.8, 4.6 and 7.3 times the freestream value for freestream Mach number cases of 5, 8 and 12, respectively, at the station corresponding to 20 degrees, Fig. (4c), a reduction beyond 50%.

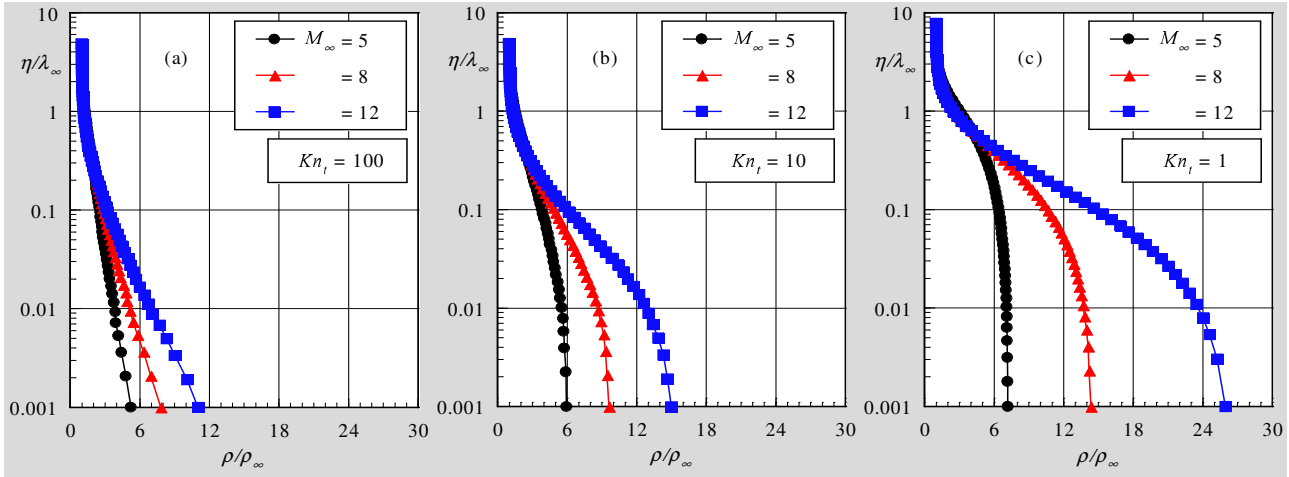


Figure 3: Density (ρ/ρ_∞) profiles along the stagnation streamline as a function of the freestream Mach number for thickness Knudsen number Kn_t of (a) 100, (b) 10 and (c) 1.

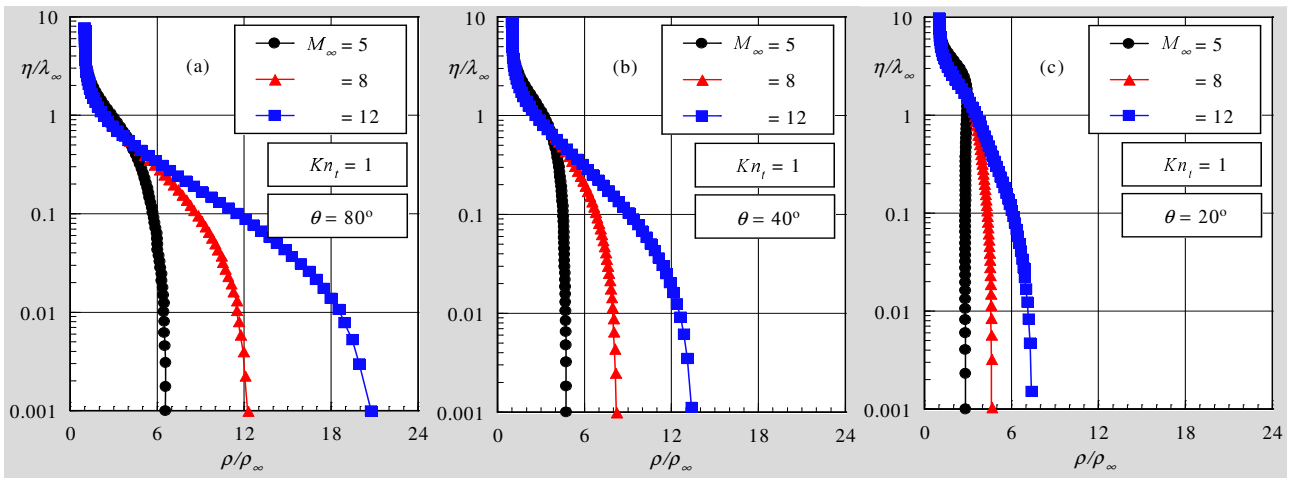


Figure 4: Density (ρ/ρ_∞) profiles along the body normal direction as a function of the freestream Mach number for thickness Knudsen number Kn_t of 1 at afterbody stations corresponding to (a) 80, (b) 40 and (c) 20 degrees.

4.3. Pressure Profile

The large amount of kinetic energy present in a hypersonic freestream is converted by molecular collisions into high thermal energy surrounding the body and by flow work into increased pressure. In this fashion, the stagnation line is a zone of strong compression, where pressure increases from the freestream to the stagnation point due to the shock wave that forms ahead of the leading edges.

Pressure profiles along the stagnation streamline are depicted as a function of the freestream Mach number M_∞ in Figs. (5a-c) for thickness Knudsen number Kn_t of 100, 10 and 1, respectively. In this set of diagrams, pressure p is normalized by the freestream pressure p_∞ . It may be recognized from these figures that there is a continuous rise in pressure from the freestream up to the stagnation

point where the maximum value is attained. Near the stagnation point, a substantial pressure increase occurs with increasing the leading edge thickness t as well as with increasing the freestream Mach number. It is apparent from these figures that the general shape of the pressure distribution profiles is preserved when the freestream Mach number increases from 5 to 12.

The extent of the upstream flowfield disturbance for pressure is significantly different from that presented by density. The domain of influence for pressure is higher than that for density and lower than that presented for temperature. Similar to the density, much of the pressure increase in the shock layer occurs after the translational kinetic temperature has reached its postshock value, as shown subsequently.

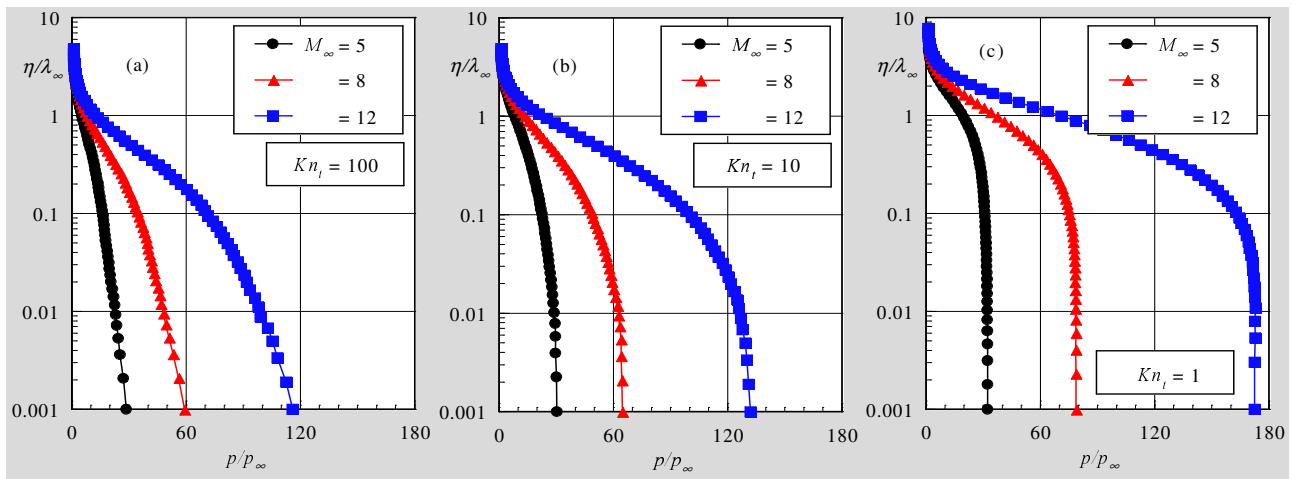


Figure 5: Pressure (p/p_∞) profiles along the stagnation streamline as a function of the freestream Mach number for thickness Knudsen number Kn_t of (a) 100, (b) 10 and (c) 1.

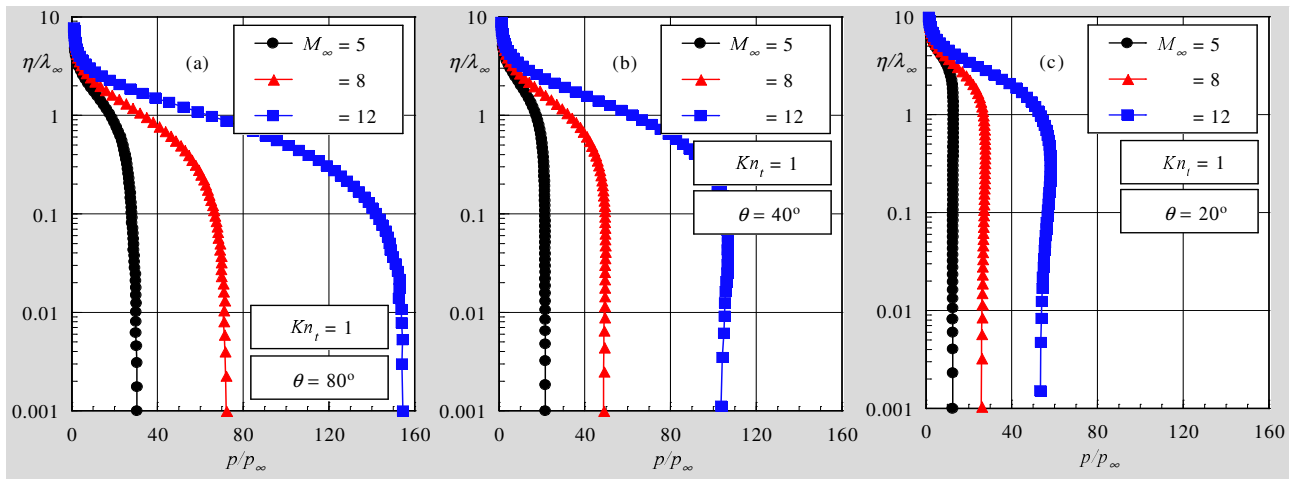


Figure 6: Pressure (p/p_∞) profiles along the body normal direction as a function of the freestream Mach number for Knudsen number Kn_t of 1 at afterbody stations corresponding to (a) 80, (b) 40 and (c) 20 degrees.

Local pressure, expressed as a ratio to the freestream value, for three stations located on the afterbody surface is demonstrated in Figs. (6a-c) for the $Kn_t = 1$ case. It is apparent from these profiles that pressure is affected by the freestream Mach number rise, as was mentioned earlier. For the station corresponding to 80 degrees, Fig. (6a), the pressure variation is in excess of two orders of magnitude for the freestream Mach number of 12. In this region, close to the leading edge shoulder, the compression produces a maximum pressure that is around 30, 72, and 154 times the freestream value for freestream Mach number of 5, 8 and 12, respectively. Due to the flow

expansion along the body surface, the pressure adjacent to the surface decreases to around 12, 25 and 53 times the freestream value for freestream Mach number cases at the station corresponding to 20 degrees, as shown in Fig. (6c), a reduction below 50% in pressure from station 80 to 20 degrees.

4.4. Temperature Profile

The strong shock wave that forms ahead of a blunt leading edge at hypersonic flow converts part of the kinetic energy of the freestream air molecules into thermal energy. This thermal energy downstream of the shock wave is partitioned into increasing the translational kinetic energy of the air molecules, and into exciting of other molecular energy states such as rotation and vibration.

Representative kinetic temperature profiles along the stagnation streamline are demonstrated in Figs. (7a-c) and (8a-c) for Knudsen number Kn_t of 100 and 1, respectively, parameterized by the freestream Mach number M_∞ . Kinetic temperature profiles for Kn_t of 10 are intermediate to these two cases, and they will not be shown. In this set of pictures, temperature ratio accounts for the kinetic temperatures normalized by the freestream temperature T_∞ . It is apparent from these figures that thermodynamic non-equilibrium occurs throughout the shock layer, as shown by the lack of equilibrium of the translational and internal kinetic temperatures. Thermal non-equilibrium occurs when the temperatures associated with the translational, rotational, and vibrational modes of a polyatomic gas are different. In this context, an overall kinetic temperature is defined for a non-equilibrium gas as the weighted mean of the translational and internal temperature (Bird, 1994). The overall kinetic temperature is equivalent to the thermodynamic temperature only under thermal equilibrium conditions. It should be emphasized that the ideal gas equation of state does not apply to this temperature in a non-equilibrium situation.

Referring to Figs. (7a-c) and (8a-c), in the undisturbed freestream far from the body, the translational and internal temperatures have the same value and are equal to the thermodynamic temperature. Approaching the nose of the leading edge, the translational temperature rises to well above the rotational and vibrational temperatures and reaches a maximum value that is a function of the leading edge thickness as well as of the freestream Mach number. Since a large number of collisions is needed to excite molecules vibrationally from the ground state to the upper state, the vibrational temperature increases much more slowly than rotational temperature. Still further downstream toward the nose of the leading edge, the translational temperature decreases and reaches a value on the wall that is above the wall temperature, resulting in a temperature jump.

The substantial rise in translational kinetic temperature for blunt leading edges occurred before the density rise (see Fig. (2)). For instance, the kinetic translational temperature reaches the maximum value around a distance of one freestream mean free path from the nose of the leading edge for the $Kn_t = 1$ case with freestream Mach number of 12, while the density ratio ρ/ρ_∞ is around 2 at the same station. The translational kinetic temperature rise for blunt leading edges results from the essentially bimodal velocity distribution: the molecular sample consisting of mostly undisturbed freestream molecules with the molecules that have been affected by the shock and reflected from the body. In this scenario, the translational kinetic temperature rise is a consequence of the large velocity separation between these two classes of molecules.

Particular attention is paid to the overall kinetic temperature in the shock layer. In this respect, the overall kinetic temperature variation is taken normal to the body surface at afterbody stations corresponding to 80, 40 and 20 degrees. Figure (9a-c) depicts the overall kinetic temperature profiles at the considered positions normal to the body surface along the η -axis for the $Kn_t = 1$ case. According to these pictures, it is observed that the downstream evolution of the flow displays a smearing tendency of the shock wave due to the displacement of the maximum value for the overall kinetic temperature. Also, it may be recognized from the temperature distribution in Figs. (9a-c) that significant changes in the overall temperature profiles occur within a thin layer adjacent to the body surface for the freestream Mach number range investigated.

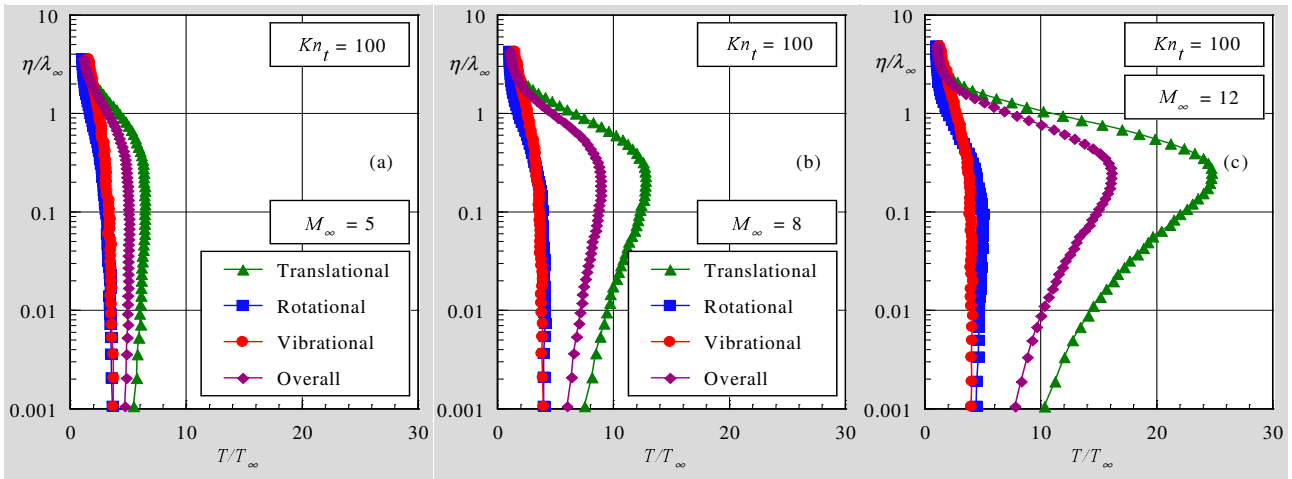


Figure 7: Kinetic temperature (T/T_∞) profiles along the stagnation streamline for thickness Knudsen number Kn_t of 100 and freestream Mach number of (a) 5, (b) 8 and (c) 12.

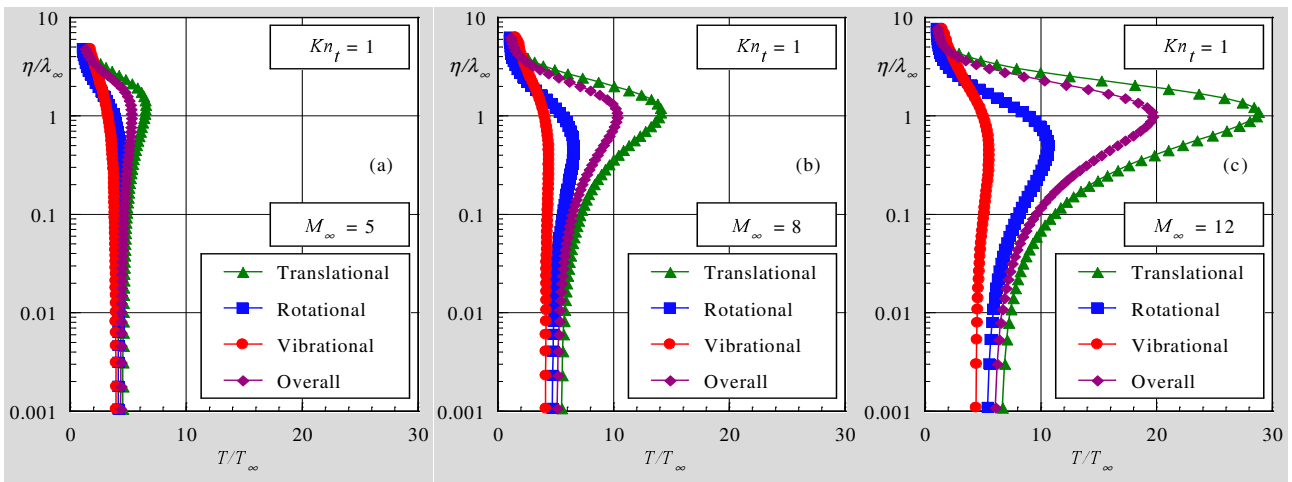


Figure 8: Kinetic temperature (T/T_∞) profiles along the stagnation streamline for thickness Knudsen number Kn_t of 1 and freestream Mach number of (a) 5, (b) 8 and (c) 12.

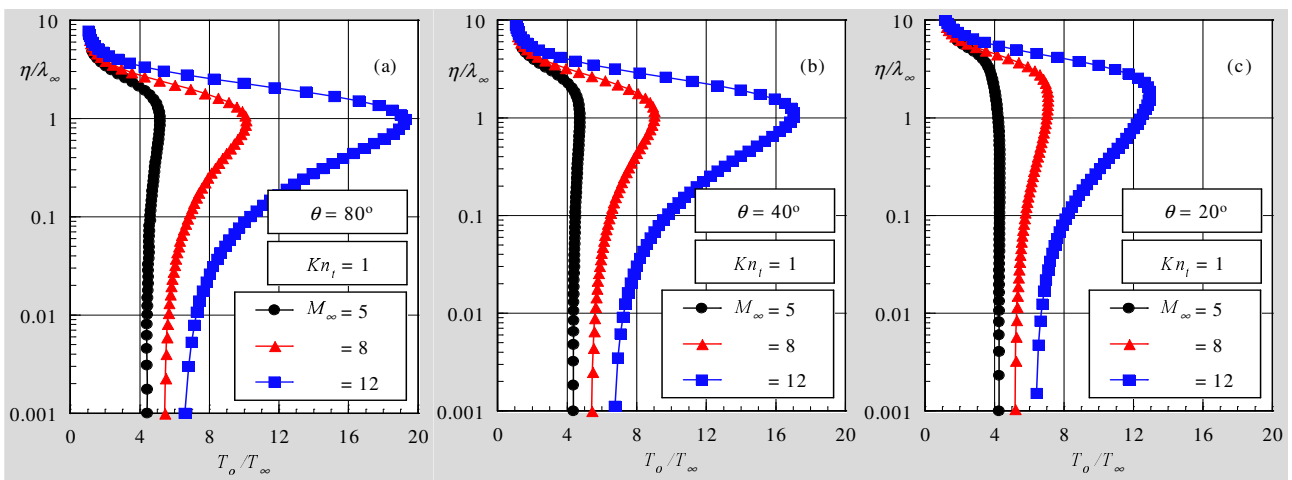


Figure 9: Overall kinetic temperature (T_o/T_∞) profiles along the body normal direction as a function of the freestream Mach number for Knudsen number Kn_t of 1 at afterbody stations corresponding to (a) 80, (b) 40 and (c) 20 degrees.

5. CONCLUDING REMARKS

Computations of a rarefied hypersonic flow on blunt leading edges have been performed by using the Direct Simulation Monte Carlo method. The calculations provided information concerning the nature of the flowfield structure about the primary properties at the vicinity of the nose and immediately adjacent to the afterbody surface for a family of contours composed by a flat face followed by a highly curved afterbody surface.

Effects of compressibility on the velocity, density, pressure, and temperature for a wide range of parameters were investigated. The freestream Mach number varied from 5 to 12. In addition to that, the flat-face thickness ranged from 0.01 to 1 of the freestream mean free path, which correspond to thickness Knudsen numbers from 100 to 1. Cases considered in this study covered the hypersonic flow from the transitional flow regime to the free molecular flow regime.

It was found that changes not only on the shape of the leading edge but also on the freestream Mach number disturbed the flowfield far upstream, as compared to the freestream mean free path, and the domain of influence decreased by reducing the nose thickness, as the leading edge became sharp, or by decreasing the freestream Mach number. Moreover, the extent of the upstream flowfield disturbance is significantly different for each one of the flow properties. The domain of influence for temperature is larger than that observed for pressure and density. Since the extent of the flowfield disturbance is significantly different for each one of the leading edge shapes, this will have important implications in problems that take into account for the gas-phase chemistry and for the gas-surface catalytic activity.

The present document has described an initial investigation of a new class of leading edges for high-altitude low-density flow. Although this investigation has taken into account for a representative number of effects, a number of improvements to a realistic leading edge design is still desirable.

6. REFERENCES

- Bird, G. A., 1981, "Monte Carlo Simulation in an Engineering Context", Progress in Astronautics and Aeronautics: Rarefied gas Dynamics, Ed. Sam S. Fisher, Vol. 74, part I, AIAA New York, pp. 239-255.
- Bird, G. A., 1989, "Perception of Numerical Method in Rarefied Gasdynamics", Rarefied gas Dynamics: Theoretical and Computational Techniques, Eds. E. P. Muntz, and D. P. Weaver and D. H. Capbell, Vol. 118, Progress in Astronautics and Aeronautics, AIAA, New York, pp. 374-395.
- Bird, G. A., 1994, "Molecular Gas Dynamics and the Direct Simulation of Gas Flows", Oxford University Press, Oxford, England, UK.
- Borgnakke, C. and Larsen, P. S., 1975, "Statistical Collision Model for Monte Carlo Simulation of Polyatomic Gas Mixture", Journal of computational Physics, Vol. 18, No. 4, pp. 405-420.
- Nonweiler, T. R. F., 1959, "Aerodynamic Problems of Manned Space Vehicles", Journal of the Royal Aeronautical Society, Vol. 63, Sept, pp. 521-528.
- Reller Jr., J. O., 1957, "Heat Transfer to Blunt Nose Shapes with Laminar Boundary Layers at High Supersonic Speeds", NACA RM-A57FO3a.
- Santos, W. F. N., 2003, "Aerodynamic Heating on Blunt Nose Shapes in Rarefied Hypersonic Flow", Proceedings of the 17th International Congress of Mechanical Engineering COBEM 2003, 10-14 Nov, São Paulo, SP, Brazil.
- Santos, W. F. N., 2004, "Surface Temperature Effects in Low-Density Flow over Flat-Nose Bodies at Hypersonic Speed. Part I: Flowfield Structure", Proceedings of the 10th Brazilian Congress of Thermal Sciences and Engineering ENCIT 2004, 29 Nov – 3 Dec, Rio de Janeiro, RJ, Brazil.
- Santos, W. F. N., 2005, "Gas-Surface Impact on Flowfield Structure of Low-Density Hypersonic Flow over Flat-Nose Bodies", Proceedings of the 18th International Congress of Mechanical Engineering COBEM 2005, 6-11 Nov, Ouro Preto, MG, Brazil.